Evidence for very early migration of the Solar System planets from the Patroclus–Menoetius binary Jupiter Trojan

David Nesvorný [1]*, David Vokrouhlický[1,2], William F. Bottke[1] and Harold F. Levison[1]

The orbital distribution of trans-Neptunian objects provides strong evidence for the radial migration of Neptune[1,2]. The outer planets' orbits are thought to have become unstable during the early stages[3], with Jupiter having scattering encounters with a Neptune-class planet[4]. As a consequence, Jupiter jumped inwards by a fraction of an au, as required from inner Solar System constraints[5,6], and obtained its current orbital eccentricity. The timing of these events is often linked to the lunar Late Heavy Bombardment that ended ~700 Myr after the dispersal of the protosolar nebula (t_0)[7,8]. Here, we show instead that planetary migration started shortly after t_0. Such early migration is inferred from the survival of the Patroclus–Menoetius binary Jupiter Trojan[9]. The binary formed at $t \lesssim t_0$[10,11] within a massive planetesimal disk once located beyond Neptune[12,13]. The longer the binary stayed in the disk, the greater the likelihood that collisions would strip its components from one another. The simulations of its survival indicate that the disk had to have been dispersed by migrating planets within $\lesssim 100$ Myr of t_0. This constraint implies that the planetary migration is unrelated to the formation of the youngest lunar basins.

Jupiter Trojans are a population of small bodies with orbits near Jupiter[14]. They hug two equilibrium points of the three-body problem, known as L_4 and L_5, with semi-major axes $a \simeq 5.2$ au, eccentricities $e < 0.15$ and inclinations $i < 40°$. Dynamical models suggest that Jupiter Trojans formed in the outer planetesimal disk between ~20 and 30 au and were implanted onto their present orbits after having a series of scattering encounters with the outer planets[12,13]. This resolves a long-standing conflict between the previous formation theories that implied $i < 10°$ and high orbital inclinations of Jupiter Trojans. The formation of Jupiter Trojans at 20–30 au is reinforced by their similarities to trans-Neptunian objects (TNOs; for example, the absolute magnitude distribution and colours[15]).

(617) Patroclus and Menoetius stand out among the 25 largest Jupiter Trojans with diameters $D > 100$ km[16,17] as a curious pair of gravitationally bound bodies with binary separation $a_B \simeq 670$ km. The formation of the Patroclus–Menoetius (P–M) binary is thought to be related to the accretion processes of small bodies themselves[10,11]. The formation model from ref. [10] implies that the P–M binary formed by capture in a dynamically cold disk at $t \sim t_0$. In ref. [11], it formed at $t < t_0$. The P–M binary provides an interesting constraint on the early evolution of the Solar System. Two conditions must be satisfied: (1) the P–M binary survived collisional grinding in its parent planetesimal disk at 20–30 au, which sets limits on the disk lifetime; (2) it survived planetary encounters during its transport from

20–30 au to 5.2 au, which sets limits on the nature of gravitational scattering events during encounters.

We first evaluated the dynamical effect of planetary encounters[18] to demonstrate the plausibility of the implantation model. To do this, we repeated numerical simulations from ref. [13] (see Methods) and monitored all encounters between disk planetesimals and planets. The planetesimals that evolved onto Jupiter Trojan orbits were selected for further use. Each selected body was then assumed to be a binary with the total mass $m_B = 1.2 \times 10^{21}$ g[19]. The initial eccentricities of binary orbits, e_B, were set to zero and the inclinations were chosen at random (assuming the isotropic orientation of the orbit-normal vectors). The binary orbits were propagated through encounters. We varied the initial binary semi-major axis, a_B, to determine how binary survival depends on the initial separation of binary components.

The binary survival is sensitive to a_B (Fig. 1). Most tight, P–M–mass binaries with $a_B < 1{,}500$ km survive, while most wide binaries with $a_B > 1{,}500$ km do not. The wide binaries become unbound during close planetary encounters, specifically when the planetocentric Hill radius of the binary, $r_{Hill,B} = q(m_B/3m_{pl})^{1/3}$, where q is the distance of the closest approach and m_{pl} is the planet mass, becomes smaller than the binary separation; that is, $r_{Hill,B} < a_B$[20]. For encounters with Jupiter, this condition works out to be $q < 1{,}680a_B$ or $q < 2.5 \times 10^6$ km for $a_B = 1{,}500$ km, which is $\simeq 0.05$ of Jupiter's Hill sphere. The removed binaries become unbound or collapse (typically because e_B becomes large). In 12–15% of cases, the bodies form a contact binary. This process may explain (624) Hektor, which is thought to be a contact binary[21]. For reference, the contact binary fraction among Jupiter Trojans is estimated to be 13–23%[22].

The survival probability of the P–M binary during planetary encounters is $\simeq 72\%$. Compared with other, nearly equal-size binaries among TNOs[23], the P–M binary with $a_B/(R_1 + R_2) \simeq 6.2$, where R_1 and R_2 are the radii of binary components, stands out as unusually compact (TNO binaries have $10 \lesssim a_B/(R_1 + R_2) < 1{,}000$). This trend is consistent with what we know because the P–M binary in the TNO region would not be spatially resolved by telescopic observations, and wide TNO binaries would not survive dynamical implantation onto a Jupiter Trojan orbit (Fig. 1). We predict that tight P–M–class binaries will be found in the TNO region when observations reach the $\simeq 0.02$ arcsec resolution needed to resolve them (the current limit with the Hubble Space Telescope is $\simeq 0.06$ arcsec[23]).

The outer planetesimal disk at 20–30 au, in which the P–M binary formed, is thought to have been massive (total estimated mass $M_{disk} \simeq 20 M_\oplus$, where $M_\oplus \simeq 6 \times 10^{27}$ g is the Earth mass), as inferred from planetary migration/instability simulations[4], the slow

[1]Department of Space Studies, Southwest Research Institute, Boulder, CO, USA. [2]Institute of Astronomy, Charles University, Prague, Czech Republic.
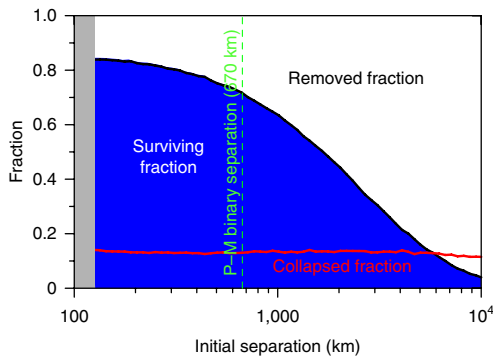*e-mail: davidn@boulder.swri.edu

Fig. 1 | Dynamical survival of binaries before their implantation onto Jupiter Trojan orbits. The P–M binaries with $a_B = 670\,km$ (green line) survive in 72% of cases, become unbound in 15% of cases and collapse into a contact binary in 13% of cases (red line). The grey area displays the conditions for which the P–M components are in contact.

migration of Neptune required to explain the inclination distribution of TNOs[24] and the capture probability of Jupiter Trojans[13]. The massive disk was subject to intense collisional grinding by impacts between planetesimals. The survival of the P–M binary in such a hostile environment is an important constraint on the disk lifetime t_{disk}, defined as the time interval between t_0 and the start of Neptune's migration.

This factor can be illustrated in the following example. Assume that a small projectile, carrying the linear momentum $p = m_i v_i$, where m_i is the projectile mass and v_i is the impact speed, hits one of the components of the P–M binary. In the limit of a fully inelastic collision, the momentum p is transferred and the binary orbit must change. The magnitude of this change, Δa_B, is $\Delta a_B / a_B \sim (m_i/m_B)(v_i/v_B)$, where v_B is the orbital speed of the binary orbit. The P–M binary has $v_B \simeq 11\,m\,s^{-1}$. Thus, to have $\Delta a_B/a_B \gtrsim 1$, the impactor mass must exceed $m_i \sim 0.01 m_B$, where we assumed $v_i = 1\,km\,s^{-1}$. The specific kinetic energy of such an impactor is $Q = m v_i^2/2 m_B \simeq 10^8\,erg\,g^{-1}$, which is ~10 times lower than the specific energy for the catastrophic disruption ($Q_D^\star \sim 10^9\,erg\,g^{-1}$ for a 100-km-class ice target[25]). We therefore see that relatively small, subcatastrophic impacts on the P–M binary can dislodge Patroclus and Menoetius from their mutual orbit.

To study this process, we used a previously developed collision code (see Methods). The collisional evolution of the outer planetesimal disk is excessive for long disk lifetimes. By 400 Myr, the disk mass is $<10 M_\oplus$ and the number of $D > 10\,km$ planetesimals drops to ~2×10^8 (Supplementary Fig. 3). The disk mass is inconsistent with that inferred from ref. [4], and the number of $D > 10\,km$ planetesimals is more than an order of magnitude below the expectation based on the Jupiter Trojan capture model[13]. These problems cannot be resolved by increasing the initial disk mass because more massive disks grind faster and the survival of the P–M binary in a more massive disk would be problematic. Here, we adopted the strong ice disruption scaling laws from ref. [25]. Weaker versions of these laws, which may be more realistic for Jupiter Trojans and TNOs, would make the problems discussed here even worse.

We found that P–M binary survival is sensitive to t_{disk} (Fig. 2). For example, for $t_{disk} = 400\,Myr$ and 700 Myr, which were the two cases suggested in the past to explain the lunar Late Heavy Bombardment (LHB)[7,8], the P–M survival probabilities are 7×10^{-5} and 2×10^{-7}, respectively. Assuming a 100% initial binary fraction and adopting the 72% dynamical survival probability computed previously, we find that having one P–M binary among the 25 largest Jupiter Trojans with $D > 100\,km$ would be a <0.002 probability event if $t_{disk} \geq 400\,Myr$. The long-lived disks can therefore be ruled out at
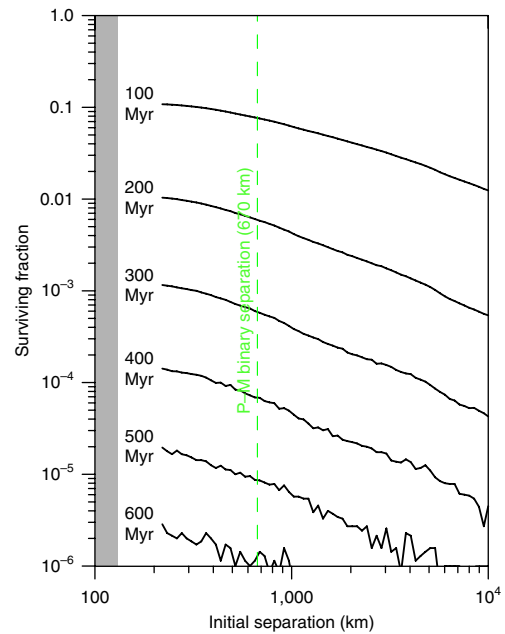

Fig. 2 | Collisional survival of binaries in the outer planetesimal disk. The surviving fraction is shown for the P–M mass binaries as a function of the initial separation and disk lifetime (labels denote t_{disk}). For the P–M binary separation and $t_{disk} \geq 400\,Myr$, the survival probability is $<10^{-4}$. The grey area displays the conditions for which the P–M components are in contact.

the 99.8% confidence level. In reality, the confidence is even greater because: (1) not all planetesimals formed as binaries; and (2) binaries that formed with $a_B > 1,000\,km$ cannot be the progenitors of the tight P–M binary (Supplementary Fig. 1).

For $t_{disk} < 100\,Myr$, the P–M survival probability against impacts is >10%, indicating that short-lived planetesimal disks may be plausible. To demonstrate this, we adopted $t_{disk} = 0$ and considered the case when Neptune migrates into the planetesimal disk immediately after t_0. The impact probability and v_i were evaluated as a function of time from the N-body simulations of Jupiter Trojan capture[13]. The changing conditions were implemented in our collisional code (see Methods), which was then used to determine the collisional survival of the P–M binary over the past 4.6 Gyr. We found that, to fit the present size distribution of Jupiter Trojans, the shape of the size distribution at $t_0 + t_{disk}$ must have been similar to the present one for $D > 10\,km$. The cumulative size distribution of Jupiter Trojans for $10 < D < 100\,km$ can be approximated by $N(>D) \propto D^{-\gamma}$ with $\gamma \simeq 2$. For $D < 10\,km$, the slope of Jupiter Trojans is shallower[26]. This is well reproduced in our simulations, where $D < 10\,km$ Jupiter Trojans are removed by disruptive impacts (Fig. 3).

The survival probability of the P–M binary is found to be 87% for $t_{disk} = 0$ (Fig. 4). Coupled with the dynamical survival from Fig. 1, the combined probability is 62%. Thus, roughly two in three primordial binaries with the P–M mass and separation would have survived to the present time (for $t_{disk} = 0$). This result can be used to estimate the occurrence rate of the P–M binaries in the original planetesimal disk. Given that P–M is the only known binary system among 25 Jupiter Trojans with $D > 100\,km$, the primordial binary occurrence rate for $a_B < 1,000\,km$ was at least 6.5% ($t_{disk} > 0$ would imply larger initial fractions). These results constitute the first constraint on the formation of tight, equal-size binaries in the outer Solar System. For comparison, about 30% of dynamically cold TNOs are thought to be wide binaries ($a_B > 1,000\,km$)[23].

The results reported here have important implications for the early evolution of the Solar System. They show that giant planet migration cannot be delayed to ~400–700 Myr after the dispersal of the protosolar
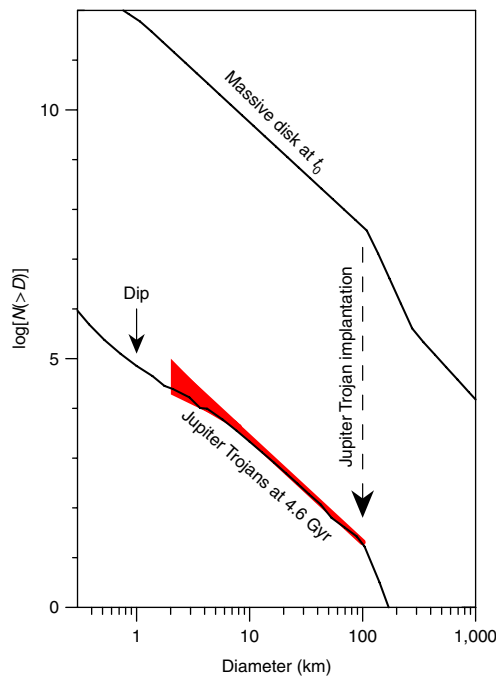
Fig. 3 | Size distribution of Jupiter Trojans. Initially, a $20M_\oplus$ planetesimal disk was placed at 20–30 au. During the disk dispersal (here assumed to have started at t_0), a small fraction of planetesimals ($\simeq 5 \times 10^{-7}$; ref. [13]) was implanted onto Jupiter Trojan orbits at 5.2 au. Here, we used our collisional code to follow the collisional grinding of Jupiter Trojans at all stages of evolution. The final population of Jupiter Trojans is a scaled-down version of the massive disk, except for $D < 10$ km, where the collisional evolution produced a dip in the size distribution. This result is consistent with observations (shown in red), which indicate a changing slope of Jupiter Trojans below ~10 km[26].

nebula (99.8% confidence). This undermines the relation between the late planetary migration/instability and LHB suggested in refs [7,8], and alleviates problems with the orbital excitation in the terrestrial planet region[5,27]. Instead, we find that the planetary migration/instability happened early, and the asteroid/comet projectiles bombarded the terrestrial worlds early as well. With $t_{disk} \lesssim 100$ Myr, the asteroid projectiles are estimated to have produced only fewer than one-tenth of large lunar craters, and fell short by a factor of ~100 to explain the formation of the Orientale/Imbrium basins at $\simeq 3.9$ billion years ago[28]. These arguments give support to the possibility that most LHB impactors originated in the terrestrial planet region[29,30].

Methods

Dynamical effects of planetary encounters on binaries. We make use of the previously published simulations of Jupiter Trojan capture[13] to evaluate the dynamical effect of planetary encounters on the P–M binary. To study capture, ref. [13] adopted three simulations of planetary instability/migration[4]. A shared property of the selected runs is that Jupiter undergoes a series of planetary encounters with an ice giant. The orbit of Jupiter evolves in discrete steps as a result of these encounters (the so-called jumping-Jupiter model). Jupiter Trojans are captured in the jumping-Jupiter model when Jupiter's Lagrange points become radially displaced by scattering events and fall into a region populated by planetesimals. The captured population was shown to provide a good match to both the orbital distribution of Jupiter Trojans and their total mass.

In ref. [13], planetesimals were initially distributed in an outer disk extending from just beyond the initial orbit of Neptune at 22 to 30 au. The outer extension of the disk beyond 30 au was ignored because various constraints indicate that a large majority of planetesimals started at <30 au (for example, ref. [31]). Also, the Jupiter Trojan capture probability from the >30 au region is exceedingly small. The simulations were performed with a modified version of the symplectic N-body integrator known as Swift[32]. All encounters of planetesimals and planets were recorded. This was done by monitoring the distance of each planetesimal
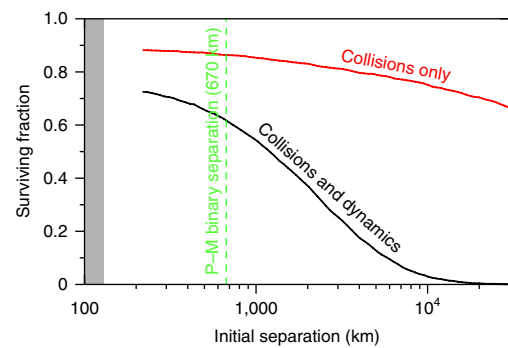

Fig. 4 | Survival of binaries in the case when the planet migration was initiated immediately after t_0 (that is, $t_{disk} = 0$). The red line shows the collisional survival of P–M mass binaries as a function of a_B. The black line combines the collisional survival with the dynamical survival from Fig. 1. It expresses our expectation for the fraction of the P–M–class binaries that should have survived to the present time ($t_{disk} > 0$ would imply lower fractions; Fig. 2). The grey area displays the conditions for which the P-M components are in contact.

from Jupiter, Saturn, Uranus and Neptune, and recording every instance when the distance dropped below $0.5R_{\mathrm{Hill},j}$, where $R_{\mathrm{Hill},j}$ are the Hill radii of planets ($j = 5$ to 8 from Jupiter to Neptune). We made sure that more distant encounters do not have any significant effect on the P–M binary. This was done by verifying that the results do not change when more distant encounters are accounted for.

The sizes of P–M binary components were obtained from the occultation observations in ref. [17]: $127\,\mathrm{km} \times 117\,\mathrm{km} \times 98\,\mathrm{km}$ for Patroclus and $117\,\mathrm{km} \times 108\,\mathrm{km} \times 90\,\mathrm{km}$ for Menoetius. A volume-equivalent spherical size corresponds to diameters $D_1 = 113\,\mathrm{km}$ for Patroclus and $D_2 = 104\,\mathrm{km}$ for Menoetius. These dimensions and the total mass $1.2 \times 10^{21}\,\mathrm{g}$ from ref. [19] imply the system density $\simeq 0.88\,\mathrm{g\,cm^{-3}}$. These are the values adopted in the main text. To study the dependence of our results on binary separation, the initial binary semi-major axis, a_B, was treated as a free parameter ($200 < a_B < 10^5\,\mathrm{km}$; for reference, the P–M binary has $a_B \simeq 670\,\mathrm{km}$). The initial orbits were assumed to be circular (eccentricity $e_B = 0$) and randomly orientated in space.

We used the model from ref. [33] to compute the effect of planetary encounters on binaries. Each binary planetesimal was traced through recorded encounters using the Bulirsch–Stoer integrator that we adapted from Numerical Recipes[34]. The Sun and other planets not having an encounter were neglected. First, we integrated the centre of mass of a binary planetesimal backwards from the closest approach until the planetocentric distance reached $3R_{\mathrm{Hill},j}$. Second, we replaced it with the actual binary and integrated forwards through the encounter. The second integration was stopped when the binary reached $3R_{\mathrm{Hill},j}$. The final binary orbit was used as the initial orbit for the next encounter. The algorithm was iterated over all recorded encounters.

Collisions between binary components were monitored. If a collision was detected, the integration was stopped and the code reported the impact speed and angle. Hyperbolic binary orbits were deemed to be unbound. The final values of a_B and e_B were recorded for the surviving binaries. We found that, in the regime corresponding to the P–M binary separation ($a_B < 1,000\,\mathrm{km}$), the final separation is generally a good proxy for the initial separation. For example, in all cases that ended with $a_B = 670\,\mathrm{km}$, only 1% of the binary orbits started with $a_B < 380\,\mathrm{km}$ or $a_B > 970\,\mathrm{km}$ (Supplementary Fig. 1). This justifies our assumption that the P–M binary started with $a_B \sim 670\,\mathrm{km}$.

Collisional evolution. The mutual orbit of a binary can be affected by small impacts into its components[35]. To study this process, we used the code known as Boulder[36,37]. The Boulder code employs a statistical algorithm to track the collisional fragmentation of planetesimal populations. Here, we briefly highlight the main points and differences with respect to refs [36,37].

For each collision, the code computes the specific impact energy Q and the critical impact energy $Q_D^\star$ (see ref. [25] for definitions). Based on the value of $Q/Q_D^\star$ and available scaling laws (for example, ref. [25]), it then determines the masses of the largest remnant and largest fragment, and the power-law size distribution of smaller fragments (for example, ref. [38]). The $Q_D^\star$ function in Boulder was set to be intermediate between impact simulations with strong[25] and weak ice[39]. To achieve this, we multiplied $Q_D^\star$ from ref. [25] by a factor f_Q, where $f_Q = 1$, 0.3 and 0.1 were used in different tests. The impact experiments with highly porous targets suggest that the $Q_D^\star$ values can be slightly higher than those found for strong ice[40]. This result reflects the dissipative properties of material porosity. We verified that using scaling laws from ref. [40] in the Boulder code gives results that are very similar to those obtained with $f_Q = 3$. We therefore tested $f_Q = 3$ as well.

The main input parameters are: (1) the initial size distribution of simulated populations; (2) the intrinsic collision probability P_i; and (3) the mean impact speed v_i. The initial size distribution can be informed from Jupiter Trojans, which are observationally well characterized down to at least 5 km[26]. For $5 \lesssim D \lesssim 100$ km, the cumulative size distribution $N(>D)$ is a power law $N(>D) \propto D^{-\gamma}$ with $\gamma \simeq 2$. Above $D \simeq 100$ km, the Jupiter Trojan size distribution bends to a much steeper slope ($\gamma \sim 6$). There are 25 Jupiter Trojans with $D > 100$ km[16]. For $D < 5$ km, the Jupiter Trojan size distribution bends to a shallower slope with $\gamma < 2$ (ref. [26]). As we discuss in the main text (Fig. 3), the shallow slope at small sizes suggests that Jupiter Trojans evolved through a stage of modest collisional grinding.

The Jupiter Trojan capture efficiency from the original planetesimal disk is well defined. Ref. [13] and our additional simulations suggest $P_{capture} = (5 \pm 2) \times 10^{-7}$ (this is a probability that an outer disk planetesimal ends up on a stable Jupiter Trojan orbit), where the error bars give the full range of values obtained in different simulations. We adopt $P_{capture} = 5 \times 10^{-7}$ in this work. To construct the size distribution of planetesimals, the Jupiter Trojan size distribution is divided by $P_{capture}$ (Supplementary Fig. 2). This gives $\simeq 6 \times 10^9$ planetesimals with $D > 10$ km. The total mass of the reconstructed population is $20 M_{\oplus}$, in agreement with ref. [4].

As for P_i and v_i, we performed two different tests. The first test was intended to replicate the collisional grinding of the outer planetesimal disk. In this case, we assumed that migrating Neptune removed the disk at t_{disk} after the dispersal of the protosolar nebula (t_0), and let the disk collisionally evolve over t_{disk}. The dynamical state of the disk was taken from ref. [41]. For example, at 300 Myr after t_0, the disk at 20–30 au is characterized by $P_i \simeq 8 \times 10^{-21}$ km^{-2} yr^{-1} and $v_i \simeq 0.4$ km s^{-1} (ref. [42]).

Collisional grinding of the outer planetesimal disk proceeds fast (Supplementary Fig. 3). For $t_{disk} > 100$ Myr, the number of $D > 10$ km bodies is reduced at least tenfold and the total mass drops to $<10 M_{\oplus}$. These results are in conflict with the current size distribution of Jupiter Trojans, the planetesimal disk mass inferred in ref. [4] and other constraints. The problem could potentially be resolved if we adopted a larger initial mass. We tested several possibilities along these lines. For example, we scaled up the reference size distribution by an additional factor to increase the initial mass to $>20 M_{\oplus}$. These tests failed because more massive disks grind faster and end up with $<10 M_{\oplus}$ for $t_{disk} > 100$ Myr. In other tests, we used a steeper slope for $D < 100$ km in an attempt to obtain $\gamma \simeq 2$ as a result of collisional grinding. These tests failed as well for reasons similar to those described above.

Using $f_Q > 1$ does not resolve the problems discussed above. This is mainly for two reasons. First, very large values of f_Q ($f_Q > 3$) are needed to significantly limit the effect of collisional grinding, but these values are probably too high to be realistic. Second, even if we use $f_Q > 3$, the number of $D \simeq 10$ km bodies is still reduced by a factor of ~10. This is because, for the low-speed impacts adopted here, the focusing factors can be large, and small planetesimals are lost by efficiently accreting on the largest disk bodies. Given these unresolved issues, we decided to adopt the following scheme for our nominal simulation of impacts on the P–M binary. We used the reference size distribution ($20 M_{\oplus}$ initially) and switched off the fragmentation of planetesimals ($f_Q \gg 1$) and their accretion onto large bodies. In this case, the size distribution stayed approximately the same over the whole length of the simulation. This is arguably a very conservative assumption. Other schemes would require that the initial population was larger and decayed over time, implying more impacts overall.

We tested many additional initial size distributions, including $\gamma \simeq 2$ for $D^* < D < 100$ km and $\gamma < 2$ for $D < D^*$, where the transition diameter $D^* < 100$ km was taken as a free parameter. This was done to verify whether the initial paucity of small projectiles would reduce the long-term exposure of the P–M binary to orbit-changing impacts. The end-member case of these models is the one with no $D < D^*$ bodies whatsoever (perhaps because they did not form). If fragmentation is switched off in this case ($f_Q \gg 1$), the size distribution remains unchanged and fails to match the present size distribution of Jupiter Trojans for $D < D^*$. If the fragmentation is switched on ($f_Q \sim 1$), the collisional cascade acts very quickly (within $\simeq 10$ Myr) to produce a fragment tail with $\gamma \simeq 2$ below $D < D^*$ km (Supplementary Fig. 4). The survival probability of the P–M binary is nearly the same in this case as in our nominal case, where the initial size distribution was extended to $D < D^*$ km with $\gamma \simeq 2$.

The second set of simulations with Boulder was done under the assumption that the outer planetesimal disk was dispersed by Neptune immediately after t_0 (that is, $t_{disk} = 0$). The disk was assumed to have started dynamically cold ($e \simeq 0$ and $i \simeq 0$) or hot (Rayleigh distributions in e and i). It was gradually excited after t_0, on a timescale of 10–30 Myr, by migrating Neptune. The Öpik algorithm[43,44] and simulations reported in ref. [13] were used to compute P_i and v_i as a function of time (Supplementary Fig. 5). We selected planetesimals that became captured as Jupiter Trojan and monitored their collision probabilities and impact velocities with all other planetesimals. The P_i and v_i values were computed each δt by averaging over the selected planetesimals, where $\delta t = 1$ Myr during the initial stages, when P_i and v_i change quickly, and $\delta t = 10$–100 Myr later on. After approximately 200 Myr past t_0, the collision evolution of Jupiter Trojans is dominated by impacts among Jupiter Trojans. After this transition, $P_i = 7 \times 10^{-18}$ km^{-2} yr^{-1} and $v_i = 4.6$ km s^{-1} (ref. [45]).

Impacts on the P–M binary. The binary module in Boulder[37] accounts for small, non-disruptive impacts on binary components, and computes the binary orbit

change depending on the linear momentum of impactors. For each impact, the change of orbital speed, $\mathbf{v}_B = \mathbf{v}_2 - \mathbf{v}_1$, where $\mathbf{v}_1$ and $\mathbf{v}_2$ are the velocity vectors of components, is computed from the conservation of the linear momentum. This gives:

$$\delta \mathbf{v}_B = \frac{m_i}{m_2 + m_i}\left(\frac{1}{2}\mathbf{v}_i - \frac{m_1}{m_B}\mathbf{v}_B\right) \tag{1}$$

for an impact on the secondary, and:

$$\delta \mathbf{v}_B = -\frac{m_i}{m_1 + m_i}\left(\frac{1}{2}\mathbf{v}_i + \frac{m_2}{m_B}\mathbf{v}_B\right) \tag{2}$$

for an impact on the primary, where m_1 and m_2 are the primary and secondary masses, $m_B = m_1 + m_2$, and m_i and $\mathbf{v}_i$ are the impactor's mass and velocity. The first term in equations (1) and (2) corresponds to the transfer of the linear momentum. The factor 1/2 stands for the contribution of the impactor's linear momentum to the translational motion (as averaged over all impact geometries). The rest of the linear momentum is consumed by the spin vector change of the impacted binary component. Note that this assumes that all collisions are completely inelastic. A larger yield would occur if it is established that the escaping ejecta affect the linear momentum budget[46], but we do not consider this effect here.

The impact velocity vectors were assumed to be randomly oriented in the reference frames of binaries. We also factored in that impacts can happen at any orbital phase and averaged the binary orbit changes over the orientation and phase. The changes of orbital elements, δa_B and δe_B, were computed from:

$$\frac{\delta a_B}{a_B} = \pm \frac{1}{\sqrt{3}}\frac{m_i v_i}{m_B v_B} \tag{3}$$

and:

$$\delta e_B = \pm \frac{1}{2}\sqrt{\frac{5}{6}}\eta \frac{m_i v_i}{m_B v_B} \tag{4}$$

where v_i and v_B are the moduli of $\mathbf{v}_i$ and $\mathbf{v}_B$, and $\eta^2 = 1 - e_B^2$. The $\pm$ sign in front of the right-hand sides indicates that the individual changes can be positive or negative. Equations (3) and (4) were implemented in the Boulder code. A similar expression can be obtained for inclinations[36], but we do not follow the inclination changes here.

References

1. Hahn, J. M. & Malhotra, R. Neptune's migration into a stirred-up Kuiper belt: a detailed comparison of simulations to observations. *Astron. J.* **130**, 2392–2414 (2005).
2. Levison, H. F., Morbidelli, A., Van Laerhoven, C., Gomes, R. & Tsiganis, K. Origin of the structure of the Kuiper belt during a dynamical instability in the orbits of Uranus and Neptune. *Icarus* **196**, 258–273 (2008).
3. Tsiganis, K., Gomes, R., Morbidelli, A. & Levison, H. F. Origin of the orbital architecture of the giant planets of the Solar System. *Nature* **435**, 459–461 (2005).
4. Nesvorný, D. & Morbidelli, A. Statistical study of the early Solar System's instability with four, five, and six giant planets. *Astron. J.* **144**, 117 (2012).
5. Agnor, C. B. & Lin, D. N. C. On the migration of Jupiter and Saturn: constraints from linear models of secular resonant coupling with the terrestrial planets. *Astrophys. J.* **745**, 143 (2012).
6. Morbidelli, A., Brasser, R., Gomes, R., Levison, H. F. & Tsiganis, K. Evidence from the asteroid belt for a violent past evolution of Jupiter's orbit. *Astron. J.* **140**, 1391–1401 (2010).
7. Gomes, R., Levison, H. F., Tsiganis, K. & Morbidelli, A. Origin of the cataclysmic Late Heavy Bombardment period of the terrestrial planets. *Nature* **435**, 466–469 (2005).

8. Bottke, W. F. et al. An Archaean heavy bombardment from a destabilized extension of the asteroid belt. *Nature* **485**, 78–81 (2012).

9. Merline, W. J. et al. S/2001 (617) 1. *Int. J. Astron. Union Circ.* **7741**, 2 (2001).

10. Goldreich, P., Lithwick, Y. & Sari, R. Formation of Kuiper-belt binaries by dynamical friction and three-body encounters. *Nature* **420**, 643–646 (2002).

11. Nesvorný, D., Youdin, A. N. & Richardson, D. C. Formation of Kuiper belt binaries by gravitational collapse. *Astron. J.* **140**, 785–793 (2010).

12. Morbidelli, A., Levison, H. F., Tsiganis, K. & Gomes, R. Chaotic capture of Jupiter's Trojan asteroids in the early Solar System. *Nature* **435**, 462–465 (2005).

13. Nesvorný, D., Vokrouhlický, D. & Morbidelli, A. Capture of Trojans by jumping Jupiter. *Astrophys. J.* **768**, 45 (2013).

14. Emery, J. P., Marzari, F., Morbidelli, A., French, L. M. & Grav, T. in *Asteroids IV* 203–220 (Univ. Arizona Press, Tucson, 2015).

15. Fraser, W. C., Brown, M. E., Morbidelli, A., Parker, A. & Batygin, K. The absolute magnitude distribution of Kuiper belt objects. *Astrophys. J.* **782**, 100 (2014).

16. Grav, T. et al. WISE/NEOWISE observations of the Jovian Trojans: preliminary results. *Astrophys. J.* **742**, 40 (2011).

17. Buie, M. W. et al. Size and shape from stellar occultation observations of the double Jupiter Trojan Patroclus and Menoetius. *Astron. J.* **149**, 113 (2015).

18. Parker, A. H. & Kavelaars, J. J. Destruction of binary minor planets during Neptune scattering. *Astrophys. J.* **722**, L204–L208 (2010).

19. Mueller, M. et al. Eclipsing binary Trojan asteroid Patroclus: thermal inertia from Spitzer observations. *Icarus* **205**, 505–515 (2010).

20. Agnor, C. B. & Hamilton, D. P. Neptune's capture of its moon Triton in a binary-planet gravitational encounter. *Nature* **441**, 192–194 (2006).

21. Marchis, F. et al. The puzzling mutual orbit of the binary Trojan asteroid (624) Hektor. *Astrophys. J.* **783**, L37 (2014).

22. Sonnett, S., Mainzer, A., Grav, T., Masiero, J. & Bauer, J. Binary candidates in the Jovian Trojan and Hilda populations from NEOWISE light curves. *Astrophys. J.* **799**, 191 (2015).

23. Noll, K. S., Grundy, W. M., Chiang, E. I., Margot, J.-L. & Kern, S. D. in *The Solar System Beyond Neptune* 345–363 (Univ. Arizona Press, Tucson, 2008).

24. Nesvorný, D. Evidence for slow migration of Neptune from the inclination distribution of Kuiper belt objects. *Astron. J.* **150**, 73 (2015).

25. Benz, W. & Asphaug, E. Catastrophic disruptions revisited. *Icarus* **142**, 5–20 (1999).

26. Wong, I. & Brown, M. E. The color-magnitude distribution of small Jupiter Trojans. *Astron. J.* **150**, 174 (2015).

27. Kaib, N. A. & Chambers, J. E. The fragility of the terrestrial planets during a giant-planet instability. *Mon. Not. R. Astron. Soc.* **455**, 3561–3569 (2016).

28. Nesvorný, D., Roig, F. & Bottke, W. F. Modeling the historical flux of planetary impactors. *Astron. J.* **153**, 103 (2017).

29. Bottke, W. F., Levison, H. F., Nesvorný, D. & Dones, L. Can planetesimals left over from terrestrial planet formation produce the lunar Late Heavy Bombardment? *Icarus* **190**, 203–223 (2007).

30. Morbidelli, A. et al. The timeline of the lunar bombardment: revisited. *Icarus* **305**, 262–276 (2018).

31. Gomes, R. S., Morbidelli, A. & Levison, H. F. Planetary migration in a planetesimal disk: why did Neptune stop at 30 AU? *Icarus* **170**, 492–507 (2004).

32. Levison, H. F. & Duncan, M. J. The long-term dynamical behavior of short-period comets. *Icarus* **108**, 18–36 (1994).

33. Nesvorný, D., Parker, J. & Vokrouhlický, D. Bi-lobed shape of Comet 67P from a collapsed binary. *Astron. J.* **155**, 246 (2018).

34. Press, W. H., Teukolsky, S. A., Vetterling, W. T. & Flannery, B. P. *Numerical Recipes in FORTRAN. The Art of Scientific Computing* (Cambridge Univ. Press, Cambridge, 1992).

35. Petit, J.-M. & Mousis, O. KBO binaries: how numerous were they? *Icarus* **168**, 409–419 (2004).

36. Morbidelli, A., Bottke, W. F., Nesvorný, D. & Levison, H. F. Asteroids were born big. *Icarus* **204**, 558–573 (2009).

37. Nesvorný, D., Vokrouhlický, D., Bottke, W. F., Noll, K. & Levison, H. F. Observed binary fraction sets limits on the extent of collisional grinding in the Kuiper belt. *Astron. J.* **141**, 159 (2011).

38. Durda, D. D. et al. Size–frequency distributions of fragments from SPH/N-body simulations of asteroid impacts: comparison with observed asteroid families. *Icarus* **186**, 498–516 (2007).

39. Leinhardt, Z. M. & Stewart, S. T. Full numerical simulations of catastrophic small body collisions. *Icarus* **199**, 542–559 (2009).

40. Jutzi, M., Michel, P., Benz, W. & Richardson, D. C. Fragment properties at the catastrophic disruption threshold: the effect of the parent body's internal structure. *Icarus* **207**, 54–65 (2010).

41. Levison, H. F., Morbidelli, A., Tsiganis, K., Nesvorný, D. & Gomes, R. Late orbital instabilities in the outer planets induced by interaction with a self-gravitating planetesimal disk. *Astron. J.* **142**, 152 (2011).

42. Morbidelli, A. & Rickman, H. Comets as collisional fragments of a primordial planetesimal disk. *Astron. Astrophys.* **583**, A43 (2015).

43. Wetherill, G. W. Collisions in the asteroid belt. *J. Geophys. Res.* **72**, 2429 (1967).

44. Greenberg, R. Orbital interactions—a new geometrical formalism. *Astron. J.* **87**, 184–195 (1982).

45. Davis, D. R., Durda, D. D., Marzari, F., Campo Bagatin, A. & Gil-Hutton, R. in *Asteroids III* 545–558 (Univ. Arizona Press, Tucson, 2002).

46. Dell'Oro, A. & Cellino, A. The random walk of Main Belt asteroids: orbital mobility by non-destructive collisions. *Mon. Not. R. Astron. Soc.* **380**, 399–416 (2007).

Acknowledgements

Author contributions

D.N. had the original idea, performed the simulations and prepared the manuscript for publication. D.V. developed the binary module in the collision code and the *N*-body code for planetary encounters. D.V., W.F.B. and H.F.L. suggested additional tests and helped to improve the manuscript.

Competing interests

The authors declare no competing interests.

Additional information

Supplementary information is available for this paper at https://doi.org/10.1038/s41550-018-0564-3.

Reprints and permissions information is available at www.nature.com/reprints.

Correspondence and requests for materials should be addressed to D.N.

Publisher's note: Springer Nature remains neutral with regard to jurisdictional claims in published maps and institutional affiliations.